(54) **Title:** AERODYNE WITH A PROPULSIVE SAUCER FOR COANDA EFFECT PROPULSION

FIG. 3
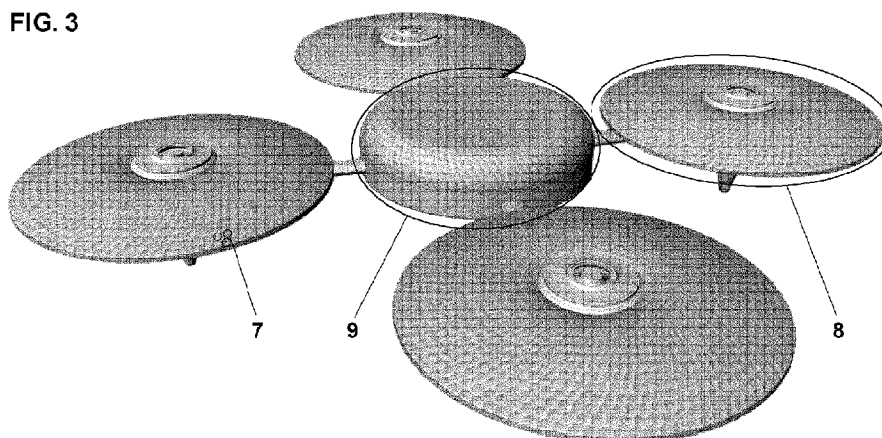
(57) **Abstract:** An aerodyne propulsion system consisting of a propulsive saucer, whose lift and maneuverability forces are governed by the fluid jet Coanda effect. The design foundation resides in the replacement of the conventional open, shaft-driven propeller by an enclosed impeller. A power system of the aerodyne is specifically designed to increase the aerodyne's endurance, based on a customized photovoltaic cell adapted to curved and/or flexible substrates. The propulsion system is used in a class of autonomous personal aerodynes designed for controllable urban flight.

AERODYNE WITH A PROPULSIVE SAUCER FOR COANDA EFFECT PROPULSION

Technical Field

[0001]   The present disclosure relates to propulsion system design, various airframe configurations, navigation and guidance implementation, and sensing platform integrations of a new class of aerodynes.

Brief Description of the Drawings

[0002]   FIG. 1 illustrates the first version of the propulsion system and its design parameterization.

[0003]   FIG. 2 illustrates the second version of the propulsion system and its design parameterization.

[0004]   FIG. 3 illustrates an aerodyne airframe with dimpled surfaces.

[0005]   FIG. 4 depicts the outlet velocity, orientation of dimple rows and inwardly inclined airfoil scheme.

[0006]   FIG. 5 is an illustration of aerodyne T4S airframe configuration.

[0007]   FIG. 6 is an illustration of aerodyne 4S02 airframe configuration.

[0008]   FIG. 7 is an illustration of aerodyne 4S01 airframe configuration.

[0009]   FIG. 8 is an illustration of aerodyne CXT8S airframe configuration.

[0010]   FIG. 9 is an illustration of aerodyne CX8S02 airframe configuration.

[0011]   FIG. 10 is an illustration of aerodyne CX8S01 airframe configuration.

[0012]   FIG. 11 is an illustration of aerodyne T6S airframe configuration.

[0013]   FIG. 12 is an illustration of aerodyne 6S02 airframe configuration.

[0014]   FIG. 13 is an illustration of aerodyne 6S01 airframe configuration.

[0015]   FIG. 14 is an illustration of aerodyne CXT12S airframe configuration.

[0016]   FIG. 15 is an illustration of aerodyne CX12S02 airframe configuration.

[0017]   FIG. 16 is an illustration of aerodyne CX12S01 airframe configuration.

[0018]   FIG. 17 illustrates the naming convention of n-saucer aerodynes.

[0019]   FIG. 18 depicts an example of photovoltaic TFSC design applied to aerodyne T4S airframe.

[0020]   FIG. 19 is a block diagram of the Geo-referential Odometry trajectory generation, navigation and guidance.

[0021]   FIG. 20 is an illustration of the position estimation and trajectory matching process.

[0022]   FIG. 21 illustrates the UAV-GPiR (Ground-Penetrating Imaging Radar) application pertaining the internal evaluation of critical structures.

[0023]   FIG. 22 illustrates the UAV-GPiR application pertaining the detection of deeply buried settlements.

[0024]   FIG. 23 illustrates the UAV-GPiR application pertaining the detection of UXO, mines and other shallow to medium depth buried targets.

[0025]   FIG. 24 illustrates the UAV-GPiR application pertaining the search and rescue on disaster or attacked sites.

[0026]   FIG. 25 illustrates the UAV-GPiR application pertaining the evaluation of serviceability, safety and structural security of critical buildings and their sites.

[0027]   FIG. 26 is an illustration of an airframe design of the autonomous personal aerodyne.

[0028]   FIG. 27 is an illustration of an alternative airframe design of the autonomous personal aerodyne.

<u>Detailed Description of Preferred Embodiments</u>

[0029]   A detailed description of systems and methods consistent with embodiments of the present disclosure is provided below. While several embodiments are described, it should be understood that the disclosure is not limited to any one embodiment, but instead encompasses numerous alternatives, modifications, and equivalents. In addition, while numerous specific details are set forth in the following description in order to provide a thorough understanding of the embodiments disclosed herein, some embodiments can be practiced without some or all of these details. Moreover, for the purpose of clarity, certain technical material that is known in the related art has not been described in detail in order to avoid unnecessarily obscuring the disclosure.

[0030]   The Coandă Effect-based propulsion and lift systems emerged in the VTOL aircraft world as a synergy of two traditional methods widely used to create lift and thrust, i.e. the fixed-wing design combined with the upper propeller creating lift through an airstream adherent over convex outer surfaces.

[0031]   The propulsion system disclosed here is quite dissimilar from previous Coandă Effect-based UAV solutions and is expected to enable superior aerodynamic performance, stability and payload capacity. These are achieved by generating lift and maneuverability forces in a more effective manner. Additionally, it offers an airframe that is virtually invulnerable to obstacle or debris impact and is able to hold altitude without being damaged in hostile environments.

[0032]   The foundation of the enhanced propulsion design disclosed here is the replacement of the traditional open, shaft driven propeller by an enclosed impeller, to enable the Coandă Effect, eliminate all of the mechanical disadvantages of an open rotor and to provide safe, quiet, responsive, FOD-resistant directional control.

[0033]   As schematically outlined in FIG. 1 and FIG. 2, the brushless motor (1) transfers its mechanical energy to the air through the ducted, rotating impeller (2). The air flows from the inlet (EYE) to the impeller center and out along its blades. The centrifugal force hereby increases the air velocity. In other words, the air is sucked into the impeller at the impeller EYE and flows through the impeller channels formed by the blades between the shroud and the hub. The vanes orientation drives the magnitude and direction of the discharged air velocity (FIG. 4). The air stream is pushed through the air amplifier (6), shaped as a circumferential slit between the fixed saucer airfoil (3) and the fixed shroud housing (4). Air speed is actually amplified as a result of Venturi Effect, which describes the increase of air velocity or flow rate due to the decrement of a passage cross-section area. Subsequently, Bernoulli's principle explains the increase in air speed that occurs simultaneously with a decrease in pressure. Furthermore, the air amplifier makes efficient use of Coandă Effect, which results in keeping the air jet attached to a NACA-profiled surface, when the air flow passes over the fixed saucer airfoil (3) to produce the Primary Lift. Finally, the air stream that is still stuck on the saucer airfoil follows the peripheral shape and is discharged quasi-vertically downward. In brief, the air is sucked, optimally 'packed' and energized by the impeller, amplified by the circumferential slit and clung to airfoil, due to Coandă Effect, to generate the main lift.

[0034]   The impeller's ability to increase air velocity and create flow depends mainly on the air pathway through the impeller. Vanes geometry (influence of vane orientation illustrated in FIG. 4) and outlet width are also performance-determining factors. Two principal impeller types have been considered: i) a closed, radial, curved-vane impeller providing higher efficiency, and ii) a semi-axial, radial discharge, curved-vane impeller providing a trade-off between pressure rise and flow. Both impeller types represent enhanced solutions that are more effective in terms of air transfer (suction), energizing and discharge than traditional propellers. Moreover, they provide FOD hazard control and eliminate the turbulence-related disadvantages of a propeller. Due to its compact design, the closed, radial impeller is preferred on coaxial configurations (FIG. 8, 9, 10, 14, 15 and 16).

[0035]   Alternatively, the propulsive saucer may be equipped with any impeller type, which provides an optimum balance between airflow rate and airspeed, when blowing the saucer airfoil, in order to enhance the Coandă Effect. The impeller design, type and material depend upon matching flow characteristics that will provide a superior aerodynamic performance than the propellers that are conventionally used with the selected brushless motor.

[0036]   The air amplifier (circumferential slit) (6) is optimized by fine-tuning the parameters p# (FIG. 1 and FIG. 2), i.e. the clearance between saucer airfoil (3) and shroud housing (4), and the diffusing angles of both (3) and (4) surfaces, in order to reduce the harmful potentiality.

[0037]   The fixed saucer airfoil (3) is a NACA-profiled surface that receives the airstream created by impeller and amplified when entering the airfoil, where the Coandă Effect applies and stimulates the diffusion of more air. In the same time, the Coandă Effect speeds up the air over the airfoil, and thus lowers the air pressure next to it, which in turn generates more lift in this area, creating the Primary Lift forces. In addition to being NACA-profiled, the saucer airfoil is also optimized for a favorable L/D ratio. Its surface is dimpled similarly to golf balls (FIG. 3 and FIG. 4). The dimples act as artificial turbulators and Coandă Effect enhancers, creating turbulence next to the surface and creating two layers of air going over the dimpled surfaces. The top layer is going faster than the bottom layer, i.e., air clings to the surface, which creates

more turbulence and reduces the drag. The local dimple-induced turbulence lowers the pressure on the adherent layer. This imbalance creates an additional upward force on the airfoil, i.e. the Secondary Lift. The dimples are oriented in rows along the design lines of the NACA profiles (generic dimple rows shown in FIG. 4), in the streamline direction of the outlet velocity (air V) vector (FIG. 4).

[0038]   A Tertiary Lift is produced by the pressure imbalance caused at the impeller's EYE (FIG. 1 and FIG. 2), around the air suction area. Furthermore, a Quaternary Lift is induced by the downward air discharge at the peripheral circumference, downstream of TPCP (FIG. 1 and FIG. 2).

[0039]   The propulsion airfoils may be inclined inwardly in order to improve aircraft's balance and stability. For example, a 5.0° inclination angle from the horizontal plane would determine a slight loss of lift (of only 0.4%) but would create a lift forces concurrence (FIG. 4). This inclination (α in FIG. 4) may also facilitate aircraft's seemingly possible water travel, by ensuring the concurrence of the horizontal vector components too.

[0040]   Two distinct designs of the fixed saucer airfoil are considered. The first version of surface of revolution is obtained by revolving the upper NACA profile curve (situated between leading edge and trailing edge, FIG. 1) around the impeller axis of rotation. The second version of surface of revolution is achieved by revolving the complete NACA profile curve consisting of both upper and lower curves (FIG. 2).

[0041]   Placing the saucer airfoil leading edge in the vicinity of air discharge and air amplifier imposed a set of design parameters (p# in FIG. 1 and FIG. 2), affecting the airflow characteristics and the aerodynamic performance. The geometric parameterization (p1, p2, p3, p4 in FIG. 1 and p5, p6, p7, p8 in FIG. 2) is meant to optimize the design cycle iterations, including the workflow steps related to digital (CFD) simulation, additive manufacturing and thrust testing.

[0042]   Regardless the version of the surface of revolution, the upper side of the saucer airfoil is a dimple-finished surface whose generatrix is a curve resulted from the NACA profile tangentially connected to a vertical air discharge profile (TPCP - tangential profile connection point - in FIG. 1 and FIG. 2), and whose dimples (7) act as artificial turbulators and Coandă Effect enhancers, being oriented along the generatrices (FIG. 3 and 4). The configuration resulted from the blend of NACA and air discharge profiles is meant to increase the streamline-directional cross-section of saucer airfoil, similarly to a flaps-deployed position maximizing the lift with a small increase in drag.

[0043]   Several airframe configurations have been considered. The aerodynes disclosed here are designed and built on a variable number of propulsive saucers, typically from minimum 4S to maximum 12S (T4S and CX12S02 in FIG. 17).

[0044]   The landing gear systems have been designed in three versions:
1) conical tube leg landing gear (12, and FIG. 7, 10, 13 and 16);
2) fixed claw landing gear (11, and FIG. 6, 9, 12 and 15); and
3) toroidal inflatable chamber landing gear (10, and FIG. 5, 8, 11 and 14).

[0045]   The toroidal inflatable chamber increases the buoyancy, functionality and/or mission autonomy; the toroidal landing gear aerodynes are designed to lift and carry a

significant weight compared to their estimated energetic consumption and also have the ability to take off, alight and loiter on water. All aerodynes illustrated here, which are built on He chambers, have similar features and operational scope.

[0046]   The fixed claw landing gear is derived from toroidal landing gear by removing the inflatable chamber.

[0047]   The aerodynes are named according to the airframe components, as listed in Table 1 and illustrated in FIG. 17.

[0048]   Table 1:

Aerodyne Mnemonic	Design Configuration
T4S	4 propulsive saucers, toroidal He inflatable chamber landing gear
4S02	4 propulsive saucers, claw landing gear (02)
4S01	4 propulsive saucers, conical tube leg landing gear (01)
CXT8S	Coaxial, 8 propulsive saucers, toroidal He inflatable chamber landing gear
CX8S02	Coaxial, 8 propulsive saucers, claw landing gear (02)
CX8S01	Coaxial, 8 propulsive saucers, conical tube leg landing gear (01)
T6S	6 propulsive saucers, toroidal He inflatable chamber landing gear
6S02	6 propulsive saucers, claw landing gear (02)
6S01	6 propulsive saucers, conical tube leg landing gear (01)
CXT12S	Coaxial, 12 propulsive saucers, toroidal He inflatable chamber landing gear
CX12S02	Coaxial, 12 propulsive saucers, claw landing gear (02)
CX12S01	Coaxial, 12 propulsive saucers, conical tube leg landing gear (01)

[0049]   Various methods have been developed to handle the UAV navigation in a GPS/communication-denied environment. Most implementations were using either Visual SLAM or Visual Odometry. However, in a real-time flight routine with SLAM-driven navigation, the computational effort imposes constraints and inherent difficulties related to processing time, computational power and memory footprint. In practice, the Visual SLAM needs more computational resources for building and maintaining a live map, and, within an equivalent iteration, its execution is slower than Visual Odometry's.

[0050]   The Geo-referential Odometry method disclosed here copes with the computational effort constraints that are conventionally encountered in UAV navigation, and proposes an MSDF approach, where the Geo-referential Odometry spatial data are integrated with data provided by GPS (when available), IMU and Barometric Altitude sensors. The Geo-referential Odometry navigation reinforces the development of a fully autonomous, intelligent aerodyne, which is built on a superior propulsion system perfectly adapted to pre-loaded mission trajectories and scenarios.

[0051]   The aerodyne is equipped with a customized flight control computer and a mission computer. The flight control computer is used to perform low-level feedback control and trajectory tracking, whereas the mission computer integrates the on-board camera with the Geo-referential Odometry system through MSDF, in order to achieve the high-level mission command and control.

[0052] First, according to the mission plans, a query will be placed to the Ground Station Computer as part of the pre-flight procedure, to obtain a set of geo-referenced map tiles, via Google Static maps API. The tiles are generated from Google Maps according to pre-planned trajectory values, and are stored corresponding to specific formats for further processing. In order to ensure effective deviation corrections, the mission's geo-referenced map tiles will be complemented by the complete set of geo-referenced tiles of contiguous areas, covering the whole spatial envelope centered on the starting location and sized to the boundary limits defined by the aerodyne's endurance.

[0053] The real-time images transmitted by the on-board cameras are received and processed to determine the current position by real-time image geo-referencing. Position is computed by applying Image-Tile Matching and Position Estimation algorithms within an open-loop 3D trajectory generator. The trajectory is computed in accordance with the mission planning, initially without considering the collision checking. A mechanism of local collision avoidance is implemented as an intermediate element between the mission path planning and the trajectory generator. The trajectory matches the mission path accurately, within a mathematical induction process, as shown in FIG. 20. The trajectory generator ensures a collision-free path from a start point to a destination point, following the geo-referenced tiles. If assumed that:

1) all positions $(P_0, P_1, ..., P_{k-1})$ are consistent with trajectory; and

2) $P_{k-1} => P_k$, i.e. the position P_k is consistent with the trajectory too, being computed from P_{k-1} by fusing the spatial data provided by the on-board sensors (IMU/barometric), and corrected by T_k tile matching and geo-referencing of the on-board image taken at t_k,

it can then be concluded that the generated trajectory is correct. The matching algorithms are typically based on greyscale conversion of both on-board images and pre-loaded tiles, and subsequent feature extraction and comparison, or cross-correlated edge extraction.

[0054] The on-board camera parameters (focal length, rotation and scale) are stored in the state vector S_k, and are used to compute the image projection matrix, i.e. the geometric transformation for image re-orientation. Then, P_k is estimated from P_{k-1} and S_k (including IMU/barometric data), and is corrected with TRV_k. Corrected P_k is also used to put forward the next tile (T_{k+1}).

[0055] By taking advantage of the highly resilient propulsion system disclosed here, the GPS/communication-denied navigation founded upon Geo-referential Odometry is not essentially dependent on IMU data. By satisfying the typical computational effort constraints and requirements, the Geo-referential Odometry navigation becomes a functional gap filler and backup to both GPS and inertial navigation systems, and can supplant either of them or both.

[0056] The block diagram of the Geo-referential Odometry navigation system is presented in FIG. 19.

[0057] The conventional propeller-driven UAVs cannot be supplied with solar power cells, for their airframes do not feature fixed airfoils or other airframe surfaces that would be large enough to be utilized as solar cell substrates. Contrariwise, the class of aerodynes listed in Table 1 and illustrated in FIG. 17 features an ideal airframe for a solar-electric UAV design. The

integration of photovoltaic cells adapted to curved and/or flexible substrates affords key functional improvements comprising:

the maximization of solar power generation in contrast to the existing versions of conventional propeller-driven UAVs;

the successive layer design, wherein the solar cells are enclosed within the airframe components, such as propulsive saucers and fuselage, by either transfer or attachment in between the rigid upper substrate and a clear, thin, dimple-finished cover (13, FIG. 18), which is attached to the rigid upper substrate and exposed to sunlight; and

improved safety, reliability and endurance.

[0058]   Various custom photovoltaic designs involving both saucer airfoils and central body are being considered. The TFSCs are enclosed within the airframe components by either transfer or attachment in between the rigid substrate and a clear, thin, dimple-shaped (FIG. 3) cover, which is exposed to sunlight. This design is supported by several methods currently available for transfer printing of either the absorber materials or the entire TFSCs onto flexible or curved rigid substrates. These transfer printing methods, in comparison to the direct deposition of TFSCs on substrates, overcome the incompatibility issues between the thermal, mechanical and chemical properties of these substrates and the fabrication conditions.

[0059]   The superior aerodynamic performance of propulsive saucers enabled the development of Autonomous Personal Air Vehicles (FIG. 26 and 27), which are built on several solar-electric design configurations (listed in Table 1) affording controllable urban flight. Their airframes include the toroidal inflatable chambers providing increased buoyancy and payload capacity.

[0060]   The Geo-referential Odometry ensures a self-controlled optimal trajectory guidance and navigation between two selectable take-off/landing points within any safe flyable urban area. The operational air space is initially mapped, decomposed into and pre-installed as a set of contiguous tiles supplied by HD aerial imagery photo-scanning, similarly to Google map's geo-referenced tiles, but of higher resolution and update frequency.

[0061]   The application scope of the aerodynes documented here ranges from integrated subsurface and aboveground 3D-imaging of critical structures to detection of underground targets with a high level of danger and security risk, supporting both Military and Civil projects and programs. The aerodynes can be integrated into various UAV-GPiR systems making up a distinct product suite for executing several applications related to National Security and Defence, comprising:

internal evaluation of critical structures (FIG. 21);

detection of deeply buried settlements (FIG. 22);

detection of UXO, mines and other shallow to medium depth buried targets (FIG. 23);

search and rescue on disaster or attacked sites (FIG. 24); and

evaluation of serviceability, safety and structural security of critical buildings and their sites (FIG. 25).

[0062]   The UAV-GPiR application pertaining the internal evaluation of critical structures consists of:

the deployment of a controllable cable-driven GPiR cart (14) on vertical and positively sloped surfaces;

a dynamically stable GPiR cart, which is cable-deployed below the propulsive saucers, where the turbulence-related disadvantages of conventional UAV propellers are eliminated; and

the ability to obtain the internal deterioration index (15), via a non-intrusive UAV-GPiR scanning.

[0063]   The UAV-GPiR application pertaining the detection of deeply buried settlements consists of:

a hybrid GPiR cart deployment system (16), wherein the GPiR antenna can be either fixed to airframe or cable-deployed/retracted for either airborne or ground-contact sensing;

the ability to operate autonomously over large remote or inaccessible areas in either individual or collaborative mode of navigation; and

the assignment of high-level mission command and control provided by the Geo-referential Odometry navigation.

[0064]   The UAV-GPiR application pertaining the detection of UXO, mines and other shallow to medium depth buried targets consists of:

the integration of a UAV-GPiR medium frequency system supporting a fixed or deployable/retractable GPiR antenna (17) for either airborne or ground-contact sensing;

the ability of scanning large areas through a collaborative mode of operation; and

the assignment of high-level mission command and control for an enhanced autonomous behaviour, provided by the Geo-referential Odometry.

[0065]   The UAV-GPiR application pertaining the search and rescue on disaster or attacked sites consists of:

the integration of a UAV-GPiR medium frequency system supporting a fixed or deployable/retractable GPiR antenna (17) for either airborne or ground-contact sensing;

the ability of scanning large areas through a collaborative mode of operation; and

the assignment of high-level mission command and control for an enhanced autonomous behaviour, provided by the Geo-referential Odometry.

[0066]   The UAV-GPiR application pertaining the evaluation of serviceability, safety and structural security of critical buildings and their sites consists of:

a hybrid GPiR cart deployment system (20), wherein the fixed GPiR antenna can be cable-deployed/retracted for either airborne or ground-contact sensing;

providing the ability to operate autonomously over large building sites in either individual or collaborative mode of navigation; and

providing the spatial qualitative and quantitative data that is used to build an accurate stratigraphic-based hydrogeological model (21), complemented with the exact topography of the extended building/structure site and the internal structural deterioration mapping.

CLAIMS

Claim 1. A propulsion system for air vehicles, wherein the improvement comprises a propulsive saucer (FIG. 1 and FIG. 2)

of which propulsion, lift and maneuverability forces are governed by the fluid jet Coandă Effect;

which affords superior aerodynamic performance, and increased buoyancy, payload capacity, endurance and performance envelope;

which serves as an integration substrate of photovoltaic cells adapted to curved and/or flexible laying surfaces; and

wherein the turbulence occurring in the vicinity of the conventional propellers is eliminated.

Claim 2. The propulsive saucer recited in Claim 1, comprising:

an attachment arm/pylon (5);

an electric motor (1) mounted on arm/pylon;

a fixed saucer airfoil (3) mounted on the stator cover of the electric motor;

a customized impeller (2);

a shroud housing (4) mounted on the upper saucer airfoil (3); and

an air amplifier (6) configured as a circumferential slit, which is optimized by fine-tuning the parameters p# (FIG. 1 and FIG. 2).

Claim 3. The fixed saucer airfoil recited in Claim 2, wherein the improvements comprise:

two distinct designs of the surfaces of revolution, wherein the first surface version is obtained by revolving the upper NACA profile curve (situated between leading edge and trailing edge, FIG. 1) around the impeller axis of rotation, whereas the second surface version is obtained by revolving the complete NACA profile curve consisting of both upper and lower curves (FIG. 2);

identifying the proper set of design parameters (p# in FIG. 1 and FIG. 2), affecting the airflow characteristics and the aerodynamic performance;

a geometric parameterization (p1, p2, p3, p4 in FIG. 1 and p5, p6, p7, p8 in FIG. 2) imposing the 3D CAD parametric modeling as solid modeling approach, and optimizing the design cycle iterations, including the workflow steps related to digital simulation, additive manufacturing and thrust testing;

its dimpled upper side, which, regardless the version of the surface of revolution, is a dimple-finished surface whose generatrix is a curve resulted from the NACA profile tangentially connected to a vertical air discharge profile (TPCP - tangential profile connection point - in FIG.

10

1 and FIG. 2), and whose dimples (7) act as artificial turbulators and Coandă Effect enhancers, being oriented along the generatrices (FIG. 3 and 'dimple row direction' in FIG. 4); and

a slight inward inclination of the saucer (FIG. 4) determining lift forces concurrence and improving aerodyne's balance, stability and maneuverability.

Claim 4. The customized impeller recited in Claim 2, wherein the improvement resides in multiple adaptive designs comprising:

a closed, radial, curved-vane impeller providing higher efficiency and, due to its compact design, being preferred on coaxial configurations (FIG. 8, 9, 10, 14, 15 and 16); or

a semi-axial, radial discharge, curved-vane impeller (FIG. 4) providing a trade-off between pressure rise and flow; or, alternatively,

any radial discharge impeller, which provides an optimum balance between airflow rate and airspeed, when blowing the saucer airfoil, in order to enhance the Coandă Effect.

Claim 5. A new and distinct class of air vehicles named 'CXTnS Aerodynes' (FIG. 17) of which design foundation resides in the replacement of the traditional open, shaft-driven propeller by an enclosed impeller, which is meant to enable the Coandă Effect affording superior aerodynamic performance, to eliminate the mechanical disadvantages of an open rotor, and to provide safe, quiet, responsive and FOD-resistant directional control.

Claim 6. The airframes of the air vehicles recited in Claim 5, comprising:

a variable number 'n' of propulsive saucers (8) attached to the bodies (9) on a modular configuration design; and

several landing gear system designs (10, 11, 12).

Claim 7. The landing gear systems recited in Claim 6, designed in three versions:

1) conical tube leg landing gear (12, and FIG. 7, 10, 13 and 16);

2) fixed claw landing gear (11, and FIG. 6, 9, 12 and 15); and

3) toroidal inflatable chamber landing gear (10, and FIG. 5, 8, 11 and 14).

Claim 8. A photovoltaic cell adapted to curved and/or flexible substrates, wherein the improvements comprise:

the utilization of the curved upper saucer surfaces as photovoltaic substrates;

maximizing the solar power generation in contrast to the existing versions of conventional propeller-driven UAVs; and

the successive layer design, wherein the solar cells are enclosed within the airframe components, such as propulsive saucers and fuselage, by either transfer or attachment in between the rigid upper substrate and a clear, thin, dimple-finished cover (13, FIG. 18), which is attached to the rigid upper substrate and exposed to sunlight.

Claim 9. A new and distinct method of 3D trajectory generation, navigation and guidance, named 'Geo-referential Odometry', which affords both individual and collaborative modes of operation, makes the air vehicles recited in Claim 5 perfectly adapted to missions and operations in a GPS/communications-denied environment, and is a functional backup to both GPS and inertial navigation systems, being able to supplant either of them or both.

Claim 10. The Geo-referential Odometry method recited in Claim 9, wherein the improvement comprises a more practical and effective computational implementation in terms of real-time processing, computational power and memory footprint, than provided by existing Visual SLAM (Simultaneous Localization and Mapping) navigation approaches.

Claim 11. The Geo-referential Odometry method of Claim 10 comprising (FIG. 19):

an interface to the real-time multi-sensor platform;

a mission planning and initialization module;

a processing module running on the mission computer in order to achieve the high-level mission command and control; and

a flight control module running on a customized flight controller utilized to perform low-level feedback control and trajectory tracking.

Claim 12. A product suite of UAV-GPiR (Unmanned Air Vehicles – Ground Penetrating Imaging Radar) integrated systems.

Claim 13. The UAV-GPiR integrated systems of Claim 12, performing applications related to National Security and Defence, comprising:

internal evaluation of critical structures (FIG. 21);

detection of deeply buried settlements (FIG. 22);

detection of UXO, mines and other shallow to medium depth buried targets (FIG. 23);

search and rescue on disaster or attacked sites (FIG. 24); and

evaluation of serviceability, safety and structural security of critical buildings and their sites (FIG. 25).

12

Claim 14. The UAV-GPiR application pertaining the internal evaluation of critical structures recited in Claim 13, wherein the improvements comprise:

the deployment of a controllable cable-driven GPiR cart (14) on vertical and positively sloped surfaces;

a dynamically stable GPiR cart, which is cable-deployed below the propulsive saucers recited in Claims 1 and 2, where the turbulence-related disadvantages of conventional UAV propellers are eliminated; and

the ability to obtain the internal deterioration index (15), via non-intrusive UAV-GPiR scanning.

Claim 15. The UAV-GPiR application pertaining the detection of deeply buried settlements recited in Claim 13, wherein the improvements comprise:

a hybrid GPiR cart deployment system (16), wherein the GPiR antenna can be either fixed to airframe or cable-deployed/retracted for either airborne or ground-contact sensing;

the ability to operate autonomously over large remote or inaccessible areas in either individual or collaborative mode of navigation; and

the assignment of high-level mission command and control provided by the Geo-referential Odometry recited in Claims 9, 10 and 11.

Claim 16. The UAV-GPiR application pertaining the detection of UXO, mines and other shallow to medium depth buried targets recited in Claim 13, wherein the improvements comprise:

the integration of a UAV-GPiR medium frequency system supporting a fixed or deployable/retractable GPiR antenna (17) for either airborne or ground-contact sensing;

the ability of scanning large areas through a collaborative mode of operation; and

the assignment of high-level mission command and control for an enhanced autonomous behaviour, provided by the Geo-referential Odometry recited in Claims 9, 10 and 11.

Claim 17. The UAV-GPiR application pertaining the search and rescue on disaster or attacked sites recited in Claim 13, wherein the improvements comprise:

a UAV-GPiR integrated system that is perfectly adapted to search and rescue operations, wherein the UAV propulsive saucers recited in Claims 1 and 2 do not induce any turbulence over the operating areas, in contrast to the conventional propeller-driven UAVs;

a fixed or deployable/retractable GPiR antenna (18) for either airborne or ground-contact sensing; and

the implementation (19) of a GPiR system enhancing the subsurface moving-target detection.

13

Claim 18. The UAV-GPiR application pertaining the evaluation of serviceability, safety and structural security of critical buildings and their sites recited in Claim 13, wherein the improvements comprise:

a hybrid GPiR cart deployment system (20), wherein the fixed GPiR antenna can be cable-deployed/retracted for either airborne or ground-contact sensing;

providing the ability to operate autonomously over large building sites in either individual or collaborative mode of navigation; and

providing the spatial qualitative and quantitative data that is used to build an accurate stratigraphic-based hydrogeological model (21), complemented with the exact topography of the extended building/structure site and the internal structural deterioration mapping.

Claim 19. A class of autonomous personal aerodynes designed in multiple airframe versions (FIG. 26 and 27), which afford controllable urban flight.

Claim 20. The autonomous personal aerodynes of Claim 19, wherein the improvements comprise:

the utilization of propulsive saucers recited in Claims 1 and 2;

an airframe design including the toroidal inflatable chamber landing gear recited in Claim 7, providing increased buoyancy and payload capacity;

the implementation of the Geo-referential Odometry navigation method recited in Claims 9, 10 and 11, ensuring a self-controlled optimal trajectory guidance and navigation between two selectable take-off/landing points within any safe flyable urban area; and

the implementation of a flight initialization routine, wherein the operational air space is initially mapped, decomposed into and pre-installed as a set of contiguous tiles supplied by HD aerial imagery photo-scanning, of higher resolution and update frequency than provided by satellite views of Google maps.
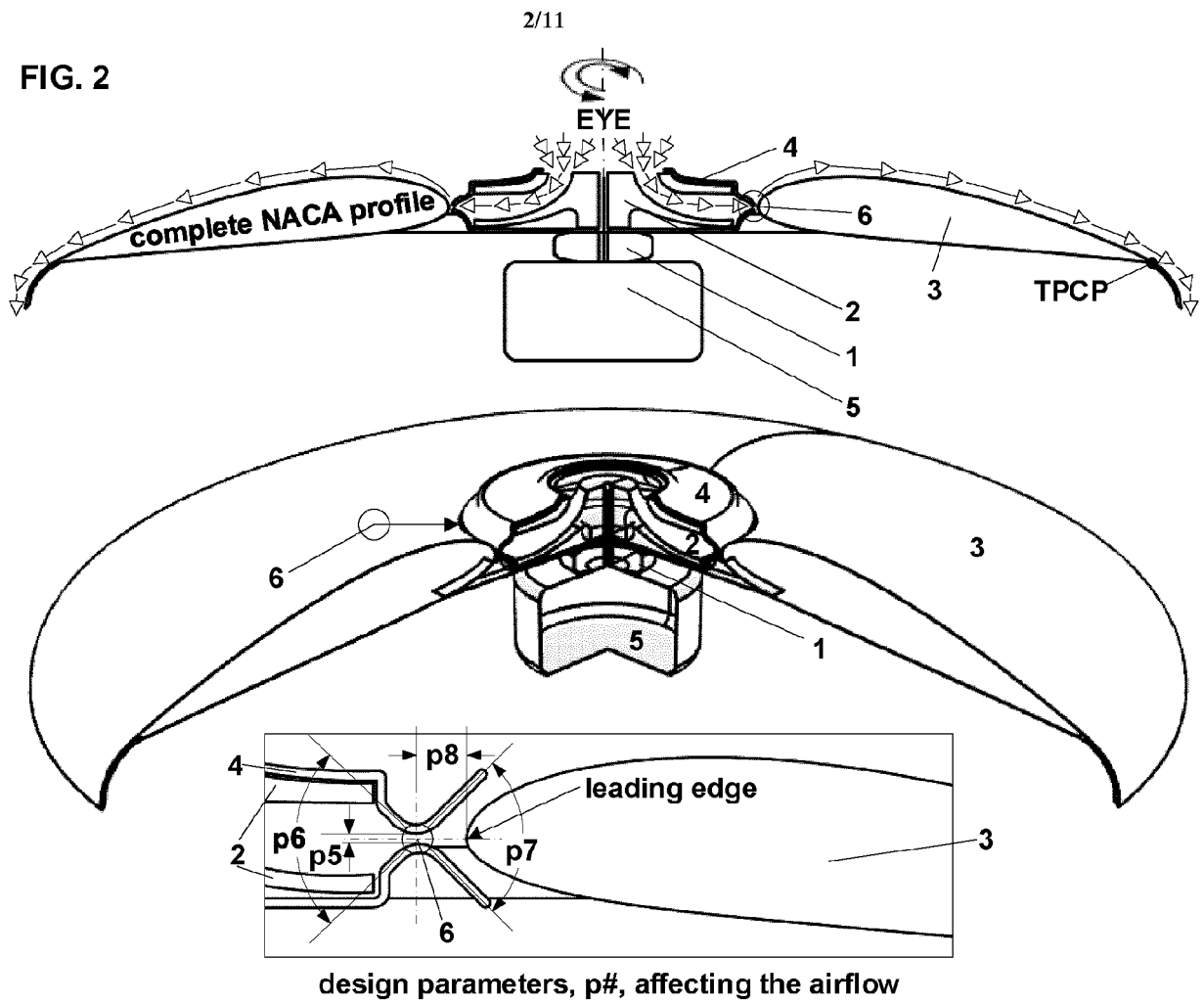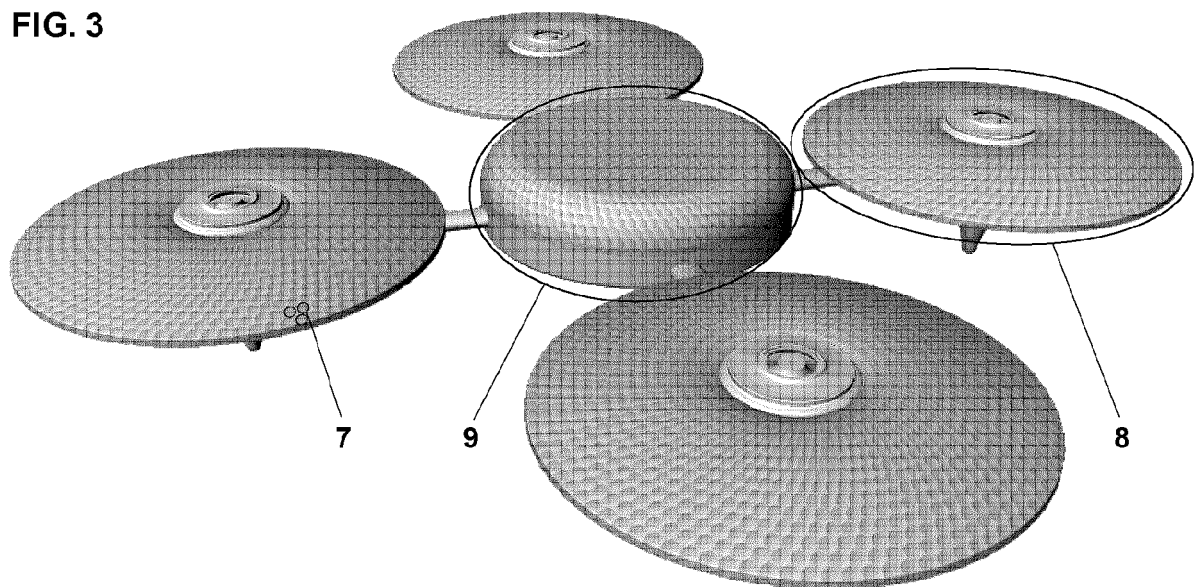
14

FIG. 1

design parameters, p#, affecting the airflow

FIG. 2

complete NACA profile

EYE

TPCP

design parameters, p#, affecting the airflow

leading edge

FIG. 3

FIG. 4

air V

dimple row direction

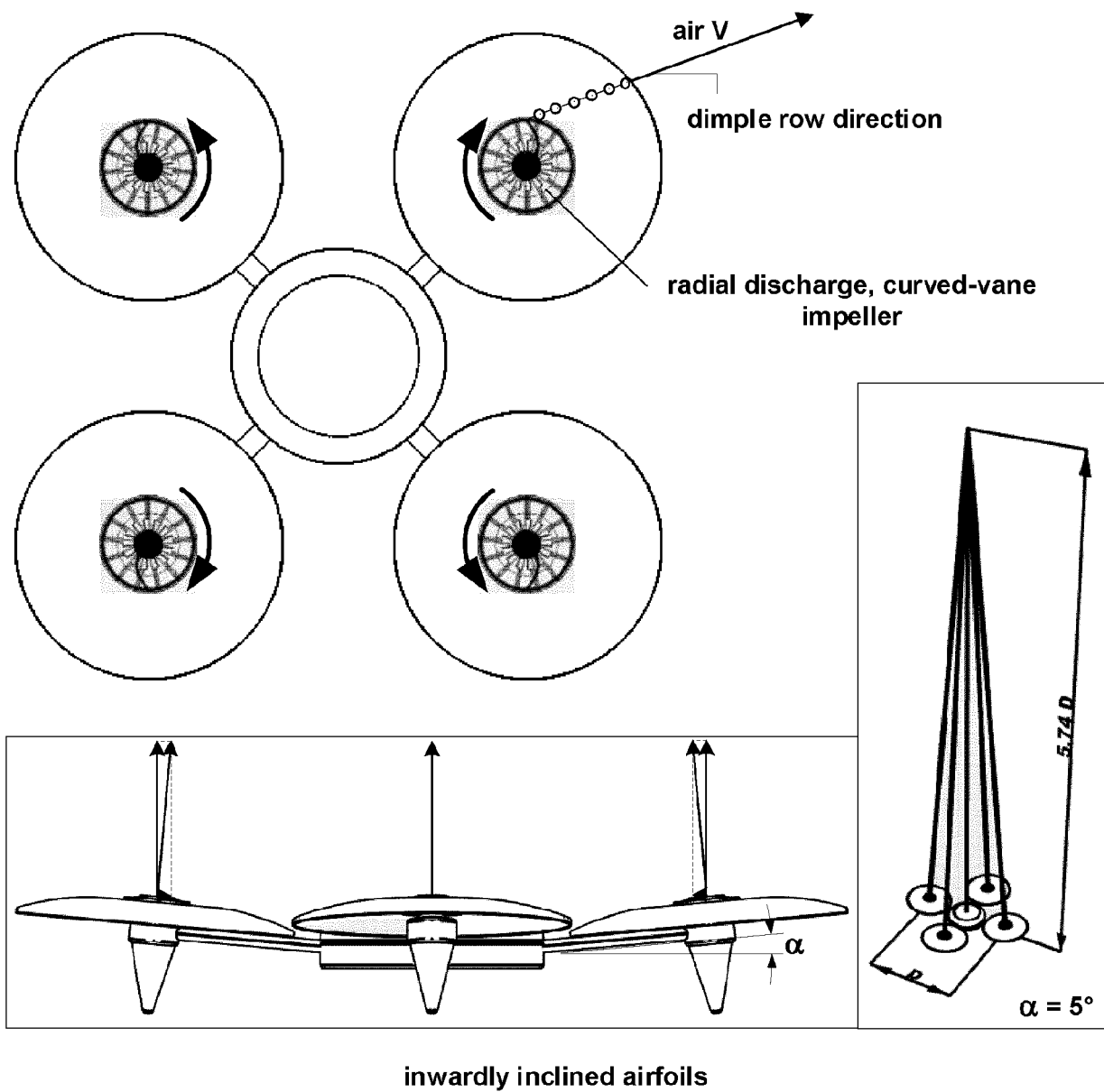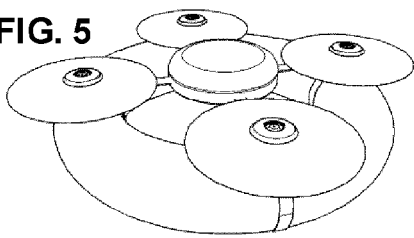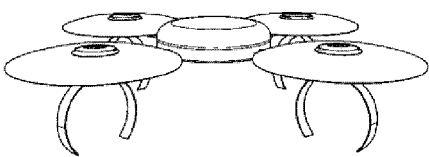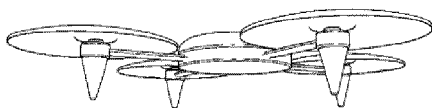radial discharge, curved-vane
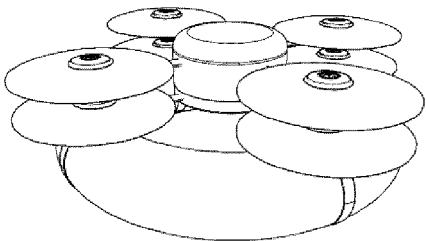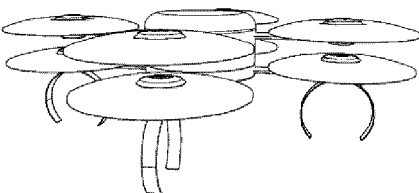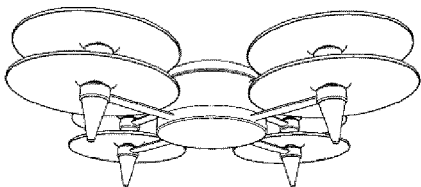impeller

5.74 D

α = 5°

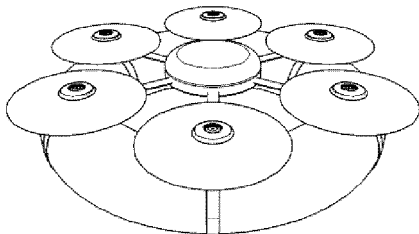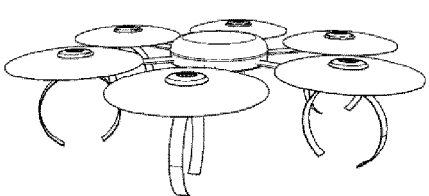inwardly inclined airfoils
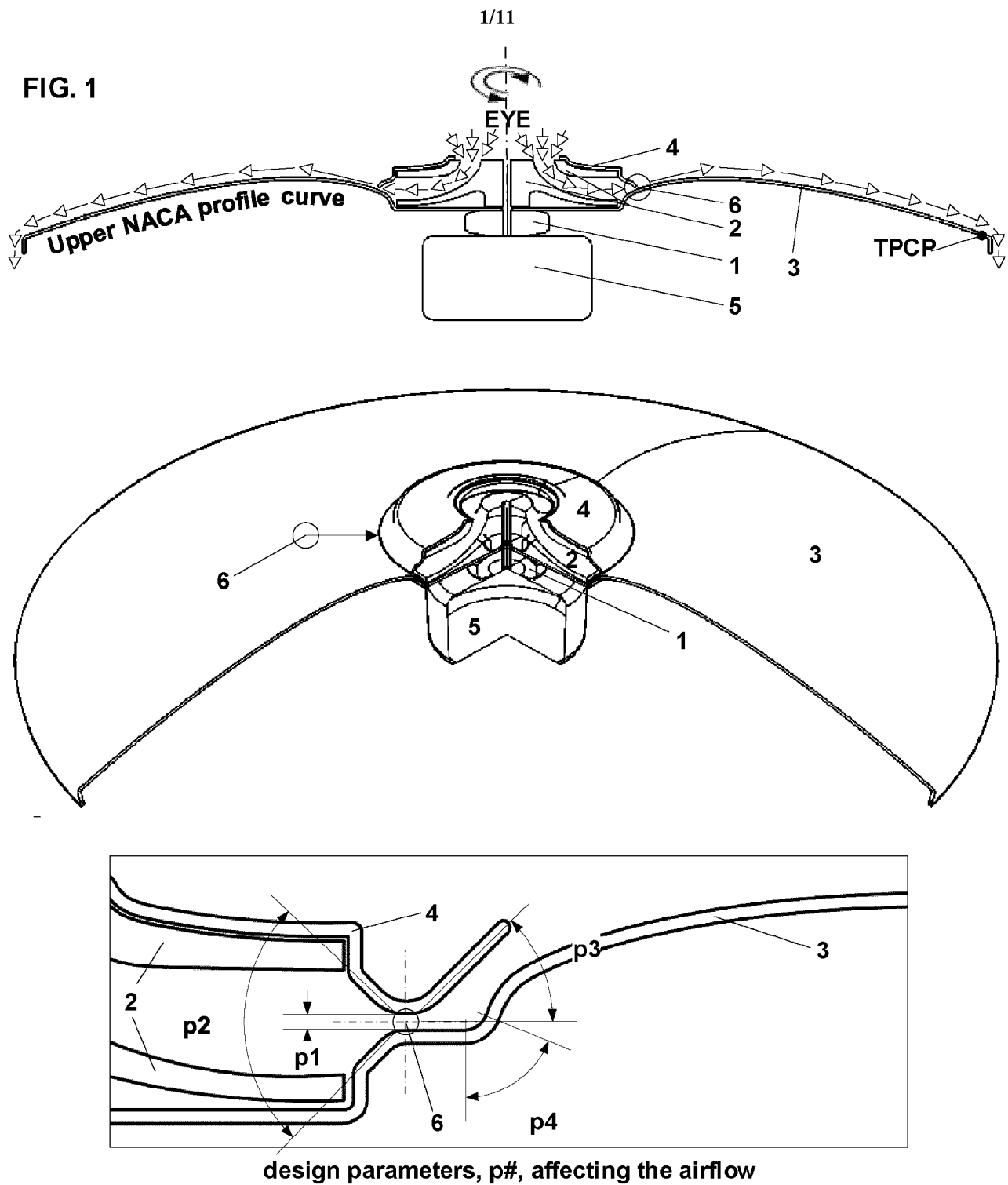
FIG. 5

FIG. 6

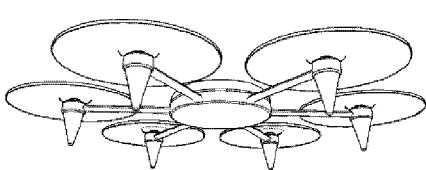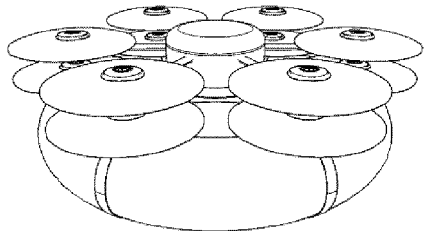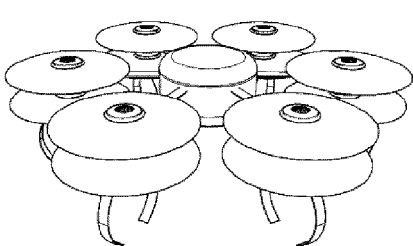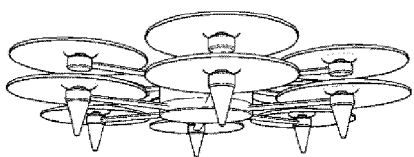FIG. 7

FIG. 8

FIG. 9

FIG. 10

FIG. 11

FIG. 12

FIG. 13

FIG. 14

FIG. 15

FIG. 16

FIG. 17

n-Saucer Aerodyne Naming Convention
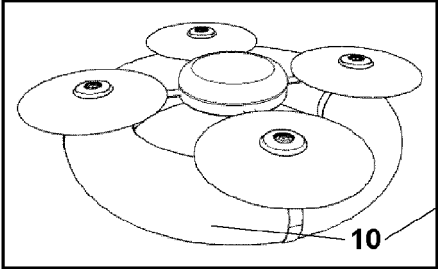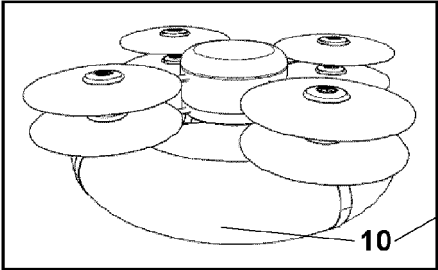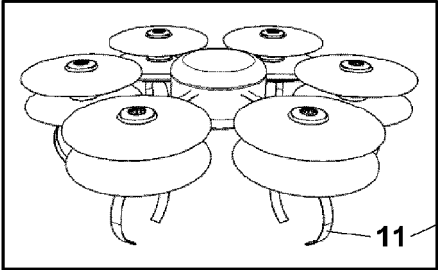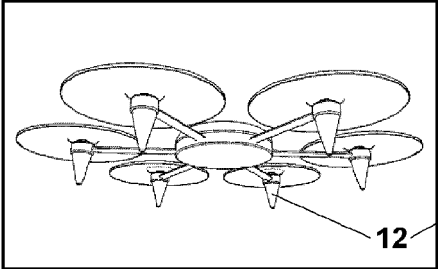
Airframe	Aerodyne Mnemonic	Design Configuration
10	T4S	T(oroidal)4S(aucers)
10	CXT8S	C(oa)X(ial)T(oroidal)8S(aucers)
11	CX12S02	C(oa)X(ial)12S(aucers)02(landing gear)
12	6S01	6S(aucers)01(landing gear)

FIG. 18

FIG. 19

FIG. 20

$[t_{k+1}, S_{k+1}, T_{k+1}, TRV_{k+1}]$

$\overrightarrow{COV}_{k+1}$

$[t_k, S_k, T_k, TRV_k]$

$\overrightarrow{COV}_k$

$[t_{k-1}, S_{k-1}, T_{k-1}, TRV_{k-1}]$

Actual vs. Estimated Position	t_k = time k S_k = UAV state vector @ t_k T_k = tile k TRV_k = tile registration vector COV_k = UAV control vector
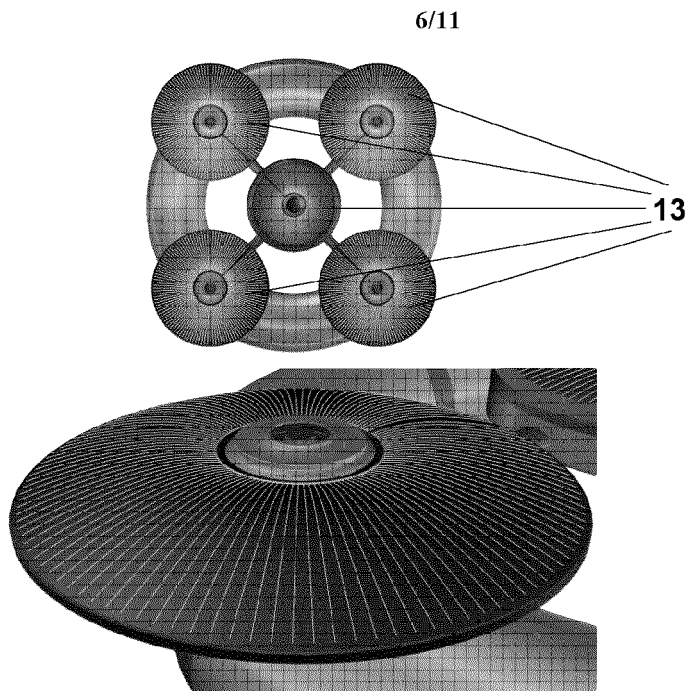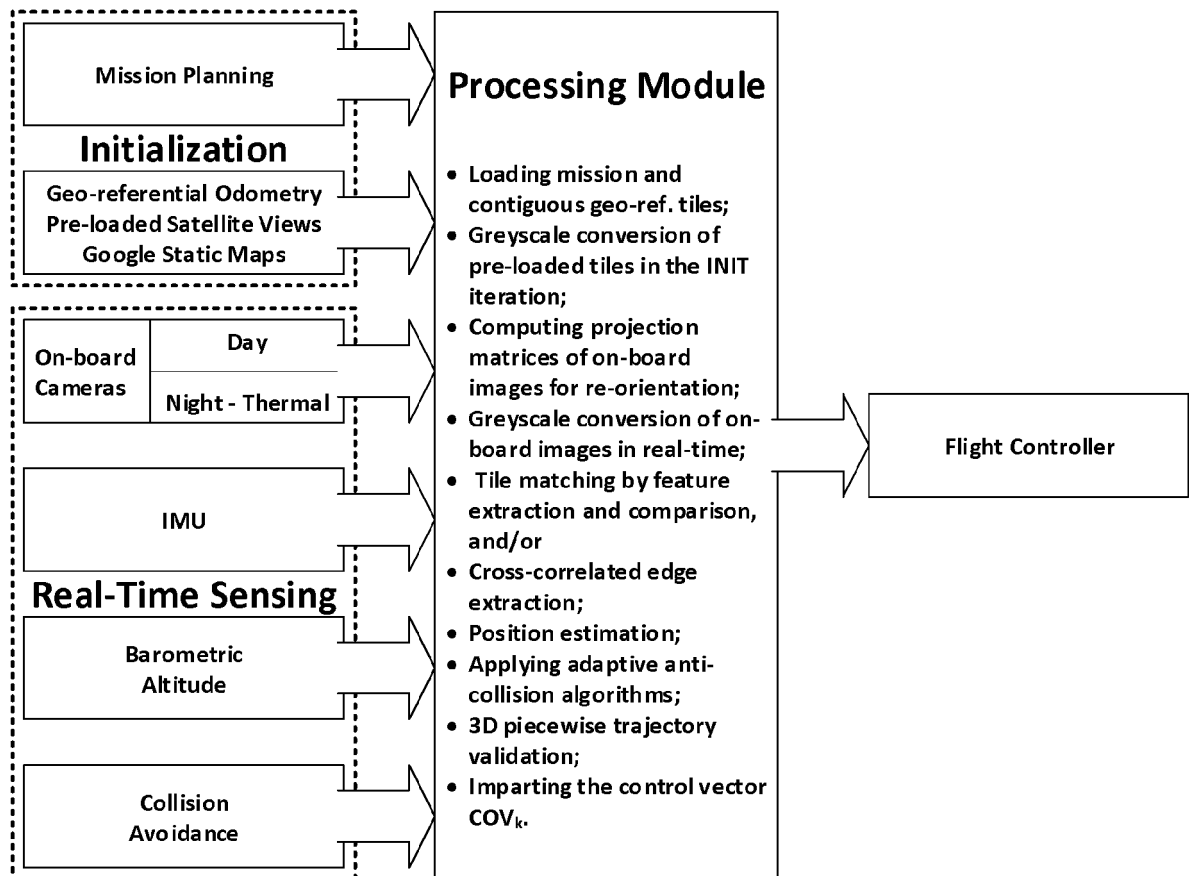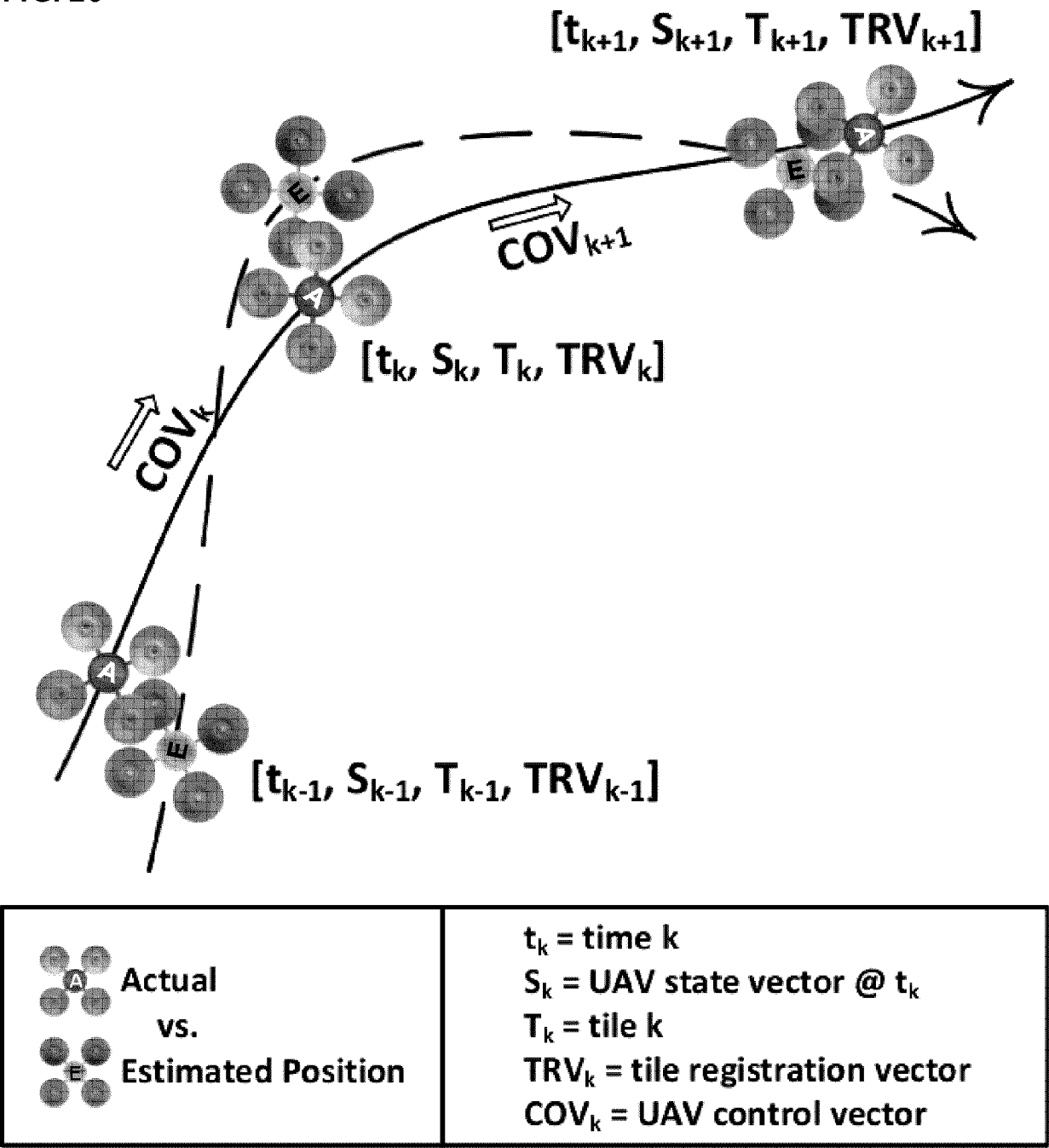
FIG. 21

FIG. 22
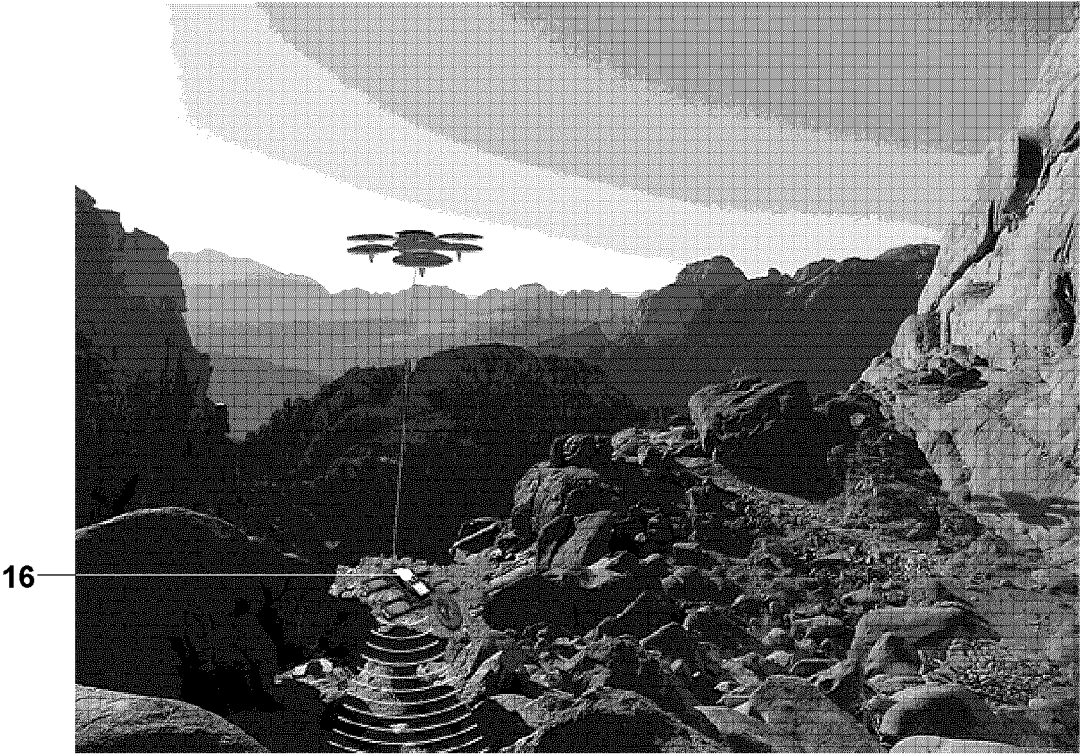
FIG. 23
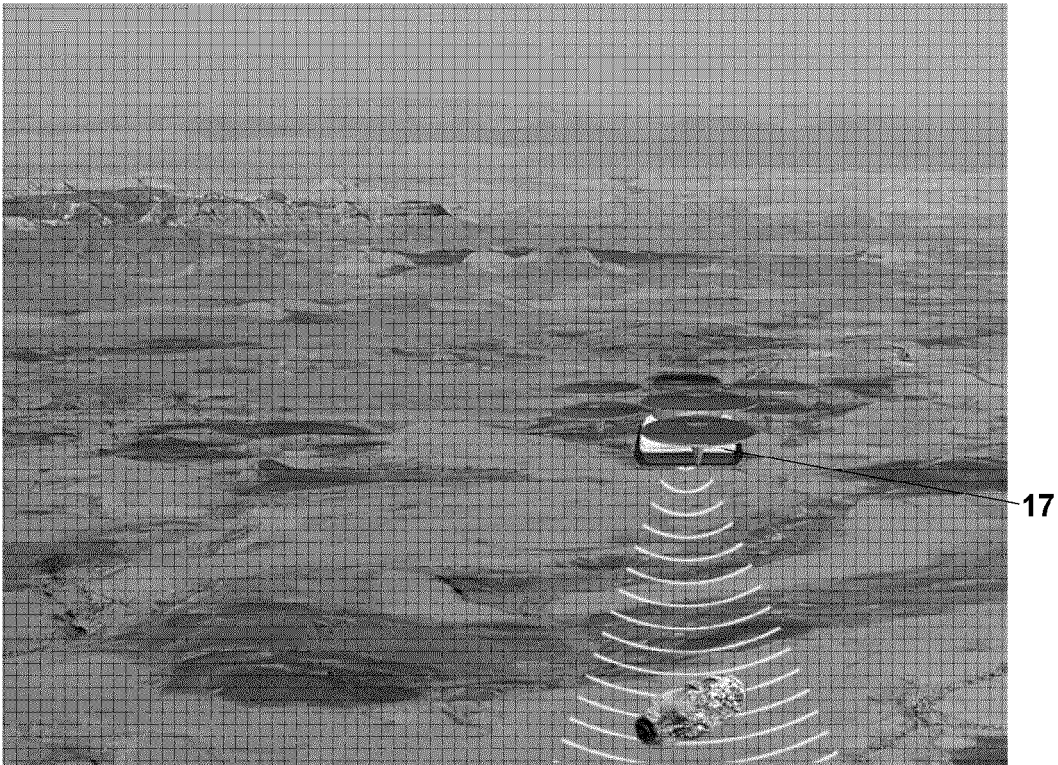
FIG. 24

FIG. 25

FIG. 26

FIG. 27

INTERNATIONAL SEARCH REPORT	International application No. **PCT/CA2018/051509**

Box No. IV   **Text of the abstract (Continuation of item 5 of the first sheet)**

An aerodyne propulsion system consisting of a propulsive saucer, whose lift and maneuverability forces are governed by the fluid jet Coanda effect. The design foundation resides in the replacement of the conventional open, shaft-driven propeller by an enclosed impeller. A power system of the aerodyne is specifically designed to increase the aerodyne's endurance, based on a customized photovoltaic cell adapted to curved and/or flexible substrates. The propulsion system is used in a class of autonomous personal aerodynes designed for controllable urban flight.

A.   CLASSIFICATION OF SUBJECT MATTER
IPC: *B64C 39/06* (2006.01) , *B64C 23/00* (2006.01) , *B64C 27/02* (2006.01) , *B64C 29/00* (2006.01) , *B64C 7/00* (2006.01)

According to International Patent Classification (IPC) or to both national classification and IPC

B. FIELDS SEARCHED

Minimum documentation searched (classification system followed by classification symbols)
IPC: B64C 39/06 (2006.01) , B64C 23/00 (2006.01) , B64C 29/00 (2006.01) , B64C 25 (2006.01)
CPC: B64C 39/001, B64C 39/003, B64C 39/006, B64C 39/064, B64C 2201/027, B64C 2201/042

Documentation searched other than minimum documentation to the extent that such documents are included in the fields searched
None

Electronic database(s) consulted during the international search (name of database(s) and, where practicable, search terms used)
QUESTEL ORBIT (FAMPAT), GOOGLE (INTERNET)
Keywords: impeller, photovoltaic, solar, saucer, annular, Coanda, multi-copter, dimple

C. DOCUMENTS CONSIDERED TO BE RELEVANT

Category*	Citation of document, with indication, where appropriate, of the relevant passages	Relevant to claim No.
X	KR20170090936 A (KIM, D) 08 August 2017 (08-08-2017) * Entire document *	1, 2, 4-6, and 19
Y		3
Y	JP2004168276 A (KAWABATA, H) 17 June 2004 (17-06-2004) * Abstract, figures 2-5 *	3
Y	US9802700 B1 (ESSARY, J.) 31 October 2017 (31-10-2017) * Figure 5 *	3
Y	DE29702492 U1 (RAUSCH, J.) 03 April 1997 (03-04-1997) * Figure 2 *	3

☑   Further documents are listed in the continuation of Box C.   ☑   See patent family annex.

*	Special categories of cited documents:	"T"	later document published after the international filing date or priority date and not in conflict with the application but cited to understand the principle or theory underlying the invention
"A"	document defining the general state of the art which is not considered to be of particular relevance		
"E"	earlier application or patent but published on or after the international filing date	"X"	document of particular relevance; the claimed invention cannot be considered novel or cannot be considered to involve an inventive step when the document is taken alone
"L"	document which may throw doubts on priority claim(s) or which is cited to establish the publication date of another citation or other special reason (as specified)	"Y"	document of particular relevance; the claimed invention cannot be considered to involve an inventive step when the document is combined with one or more other such documents, such combination being obvious to a person skilled in the art
"O"	document referring to an oral disclosure, use, exhibition or other means		
"P"	document published prior to the international filing date but later than the priority date claimed	"&"	document member of the same patent family

Date of the actual completion of the international search 20 June 2019 (20-06-2019)	Date of mailing of the international search report 05 July 2019 (05-07-2019)
Name and mailing address of the ISA/CA Canadian Intellectual Property Office Place du Portage I, C114 - 1st Floor, Box PCT 50 Victoria Street Gatineau, Quebec K1A 0C9 Facsimile No.: 819-953-2476	Authorized officer Daniel Rempel (819) 639-7893

Box No. II	Observations where certain claims were found unsearchable (Continuation of item 2 of the first sheet)

This international search report has not been established in respect of certain claims under Article 17(2)(a) for the following reasons:

1. ☐ Claim Nos.:
   because they relate to subject matter not required to be searched by this Authority, namely:

2. ☐ Claim Nos.:
   because they relate to parts of the international application that do not comply with the prescribed requirements to such an extent that no meaningful international search can be carried out, specifically:

3. ☑ Claim Nos.: 20
   because they are dependent claims and are not drafted in accordance with the second and third sentences of Rule 6.4(a).

Box No. III	Observations where unity of invention is lacking (Continuation of item 3 of first sheet)

This International Searching Authority found multiple inventions in this international application, as follows:
The claims are directed to a plurality of inventive concepts as follows:

> Group A - Claims 1-7, 19 and 20 are directed to an air vehicle;
> Group B - Claim 8 is directed to a photovoltaic cell;
> Group C - Claims 9-11 are directed to a method of 3D trajectory generation; and
> Group D - Claims 12-18 are directed to a product suite of unmanned air vehicles with ground penetrating imaging radar.

The claims must be limited to one inventive concept as set out in PCT Rule 13.

1. ☐ As all required additional search fees were timely paid by the applicant, this international search report covers all searchable claims.

2. ☐ As all searchable claims could be searched without effort justifying additional fees, this Authority did not invite payment of additional fees.

3. ☐ As only some of the required additional search fees were timely paid by the applicant, this international search report covers only those claims for which fees were paid, specifically claim Nos.:

4. ☑ No required additional search fees were timely paid by the applicant. Consequently, this international search report is restricted to the invention first mentioned in the claims; it is covered by claim Nos.:
1-7, 19, and 20

Remark on Protest
- ☐ The additional search fees were accompanied by the applicant's protest and, where applicable, the payment of a protest fee.
- ☐ The additional search fees were accompanied by the applicant's protest but the applicable protest fee was not paid within the time limit specified in the invitation.
- ☐ No protest accompanied the payment of additional search fees.

C (Continuation).   DOCUMENTS CONSIDERED TO BE RELEVANT

Category*	Citation of document, with indication, where appropriate, of the relevant passages	Relevant to claim No.
Y	LIVYA, E. et al., "Aerodynamic Analysis of Dimple Effect on Aircraft Wing", World Academy of Science, Engineering and Technology International Journal of Aerospace and Mechanical Engineering Vol:9, No:2, 2015 * Entire document *	3
A	US5351911 A (NEUMAYR, G.) 04 October 1994 (04-10-1994) * Figure 1 *	1
A	IN201841034280 A (MERUVA, R.) 28 September 2018 (28-09-2018) * Figure 4 *	7
A	CN108791850 A (XIE, X. et al.) 13 November 2018 (13-11-2018) * Figure 1 *	7

Patent Document Cited in Search Report	Publication Date	Patent Family Member(s)	Publication Date
KR20170090936A	08 August 2017 (08-08-2017)	None	
JP2004168276A	17 June 2004 (17-06-2004)	None	
US9802700B1	31 October 2017 (31-10-2017)	None	
DE29702492U1	03 April 1997 (03-04-1997)	DE19626112A1	02 January 1998 (02-01-1998)
US5351911A	04 October 1994 (04-10-1994)	None	
IN201841034280 A	28 September 2018 (28-09-2018)	None	
CN108791850A	13 November 2018 (13-11-2018)	None	